ISSN 1063-7745, Crystallography Reports, 2018, Vol. 63, No. 2, pp. 172–177. © Pleiades Publishing, Inc., 2018.
Original Russian Text © A.P. Dudka, 2018, published in Kristallografiya, 2018, Vol. 63, No. 2, pp. 190–194.

STRUCTURE OF INORGANIC COMPOUNDS

First Russian Crystallographic Congress

Accurate Refinement of the Crystal Structure of $Ba_3TaGa_3Si_2O_{14}$ from Langasite Family and Analysis of Structural Transformations Due to Isomorphous Cation Substitutions

A. P. Dudka

Shubnikov Institute of Crystallography of Federal Scientific Research Centre "Crystallography and Photonics," Russian Academy of Sciences, Moscow, 119333 Russia

e-mail: dudka@ns.crys.ras.ru

Received May 12, 2017

Abstract—An accurate structure analysis of a $Ba_3TaGa_3Si_2O_{14}$ single crystal from langasite family was performed using four X-ray diffraction data sets collected on a diffractometer equipped with a CCD area detector (sp. gr. $P321$, $Z = 1$, $\sin\theta/\lambda \le 1.35$ Å^{-1}; at 295 K $a = 8.516(1)$ Å, $c = 5.1910(6)$ Å, $R/wR = 0.58/0.56\%$, $\Delta\rho_{min}/\Delta\rho_{max} = -0.73/0.42$ e/Å^3, 4414 independent reflections; at 106 K $a = 8.5109(9)$ Å, $c = 5.1861(9)$ Å, $R/wR = 0.75/0.86\%$, $\Delta\rho_{min}/\Delta\rho_{max} = -0.81/1.06$ e/Å^3, 4382 reflections). The distinguishing feature of the $Ba_3TaGa_3Si_2O_{14}$ structure is a strong disorder of the Ga atom at the 3*f* site. Structural transformations in the series of $Ca_3TaGa_3Si_2O_{14}$–$Sr_3TaGa_3Si_2O_{14}$–$Ba_3TaGa_3Si_2O_{14}$–$Ba_3TaFe_3Si_2O_{14}$ crystals were analyzed.

DOI: 10.1134/S1063774518020049

INTRODUCTION

As has long been suggested [1, 2], the electron density (ED) determines the microscopic properties of crystals in the ground state. The energy minimization of the unit cell gives the model ED, which can be used to calculate some properties [3, 4], in particular, piezoelectric coefficients. The X-ray diffraction analysis provides experimental ED; however, the number of characteristics, which can be derived from these data, is much smaller [5]. Therefore, valuable information on the dependence of the physical properties of crystals on their structures can be obtained by performing comparative study of isomorphous substitutions in series of crystals.

Crystals of the langasite family (the $Ca_3Ga_2Ge_4O_{14}$ structure type, sp. gr. $P321$, $Z = 1$ [6, 7]) are convenient models for such analysis. First, these crystals have a wide range of well-known properties, such as optical, piezoelectric [8, 9], and multiferroic [10, 11]. Second, these crystals allow for a wide isomorphism in all four cation positions.

Let us consider the crystal structure of $Ba_3TaGa_3Si_2O_{14}$ (BTGS) (Fig. 1) prepared in this study. The first chemical element (Ba) in the formula occupies the 3*e* site at the center of a distorted Thompson polyhedron. A large cavity to the right of this polyhedron is responsible for mobility of atoms under an applied pressure or electric field and, to a large extent, determines the piezoelectric properties of the crystals [12, 13]. The atoms of two other polyhedra–Ta at the 1*a* site in

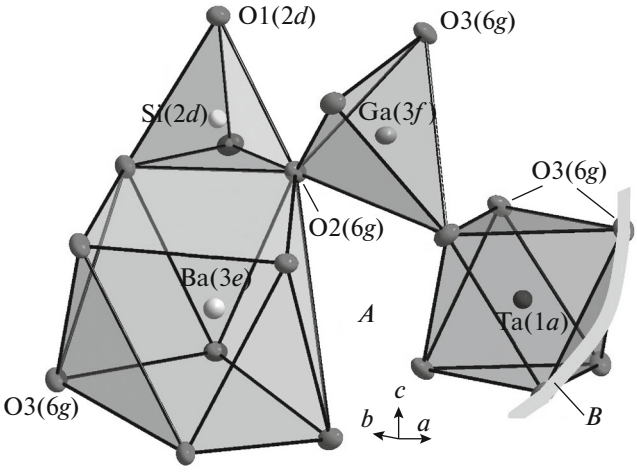

Fig. 1. Main polyhedra in the $Ba_3TaGa_3Si_2O_{14}$ structure: *A* is the cavity to the right of the 3*e* polyhedron that has an effect on the piezoelectric properties; *B* is a fragment of the Ga(3*f*)–O3(6*g*)–O3(6*g*)–Ga(3*f*) helix responsible for crystal chirality.

an octahedron and Ga at the 3*f* site in a large tetrahedron – are involved in the formation of the structural helix Ga(3*f*)–O3(6*g*)–O3(6*g*)–Ga(3*f*), which endows langasites with chirality [14, 15] and is responsible for their optical [16] and multiferroic [17] properties. The fourth polyhedron is a small Si tetrahedron, the center of which lies at the 2*d* site. This tetrahedron is very rigid and generally moves as a rigid body under applied loads.

The goal of this work was to perform an accurate investigation of the atomic structure of the BTGS crystal. The low-temperature structural data for BTGS are reported for the first time. These data were used for the comparative analysis of the crystal structures of $Ca_3TaGa_3Si_2O_{14}$ (CTGS) [18], $Sr_3TaGa_3Si_2O_{14}$ (STGS) [19], $Ba_3TaGa_3Si_2O_{14}$, and $Ba_3TaFe_3Si_2O_{14}$ (BTFS) [20].

EXPERIMENTAL

A finely-crystalline aggregate of BTGS was grown by pulling from a stoichiometric melt by the Czochralski method under a $95N_2$–$5O_2$ atmosphere. The sample used for the X-ray diffraction study was prepared from the largest (up to 3 mm) crystallites. It had the smooth surface and was optically transparent and nearly spherical. The X-ray diffraction experiments were performed at two temperatures. At both temperatures, two X-ray diffraction data sets were collected at different orientations of the sample on a Rigaku Oxford Diffraction Xcalibur S3 diffractometer equipped with a CCD area detector. The calibration [21] showed that the real temperature of the sample was 106 K in the low-temperature measurements (95 K measured with a built-in sensor) and 295 K in the room-temperature experiments. The X-ray data collection and structure-refinement statistics for the BTGS crystal are given in Table 1. The structural data were deposited at the Inorganic Crystal Structure Database (ISCD; CSD refcodes 380523 and 433692).

The integrated intensities were calculated with the CrysAlisPro program [22]. Other calculations were performed with the ASTRA program [23, 24]: the correction for thermal diffuse scattering [25] using elastic constants calculated by an ab initio method [26]; the correction of intensities for absorption by ellipsoidal samples [27]; the calibration of the diffractometer [28, 29]; the extinction correction [30, 31]; the refinement of the half-wavelength contribution [32]; the anharmonic displacement expert (the Hamilton–Fisher test) [33]; the Abrahams–Keve test [34] for comparison of the models (the normal probability plot). The final structure model was refined based on the cross-data set obtained by merging two X-ray diffraction data sets (the method of intermeasurement minimization or experimental comparison) [35].

RESULTS AND DISCUSSION

Crystals of BTGS appeared to be the most difficult to study in the CTGS–STGS–BTGS series. Attempts to grow large well-faceted single crystals of BTGS failed. There were difficulties with the selection of samples for X-ray diffraction. Nevertheless, high relative precision and good reproducibility of X-ray diffraction results were achieved. In the BTGS structure, the cation positions, particularly Ga(3*f*), are highly disordered. An anharmonic tensor up to the sixth order was applied for the first time (for the langasite family) to describe this disorder. At 295 K the transformation from a fourth-order tensor to a six-order tensor for Ga(3*f*) and an increase in the number of parameters from 79 to 104 led to an improvement of the model fitting from $R1(|F|)/wR2(|F|) = 0.664/0.670$ to 0.578/0.562%, which is significant at a level of 0.9999 [33], $\Delta\rho_{min}/\Delta\rho_{max}$ being changed from −0.60/1.17 to −0.73/0.42 e/Å^3. At 106 K the extension of the model resulted in an even more significant improvement of the fitting. Atomic coordinates, equivalent thermal displacement parameters, and ellipsoidality parameters [19] are given in Table 2.

Let us consider the results of isomorphous substitutions in the series CTGS → STGS → BTGS → BTFS. The first three compounds are generated by the replacement of a divalent cation at the 3*e* site, with coordination number 8, by larger cations: Ca → Sr → Ba with r(Ca/Sr/Ba) = 1.12/1.26/1.42 Å. The fourth compound is derived by subsequent substitution Ga(3*f*) → Fe(3*f*), which is also accompanied by an increase in the ion size: $r(Ga^{3+}_{IV}/Fe^{3+}_{IV}) = 0.47/0.49$ Å. An evident increase in the unit-cell volume ~283 → 303 → 326 → 330 Å^3 is accompanied by both an increase and a decrease in the volumes of the polyhedra V (Fig. 2). The most substantial change is the mobility of atoms along the 2 axes (the *a* axis of the unit cell) (Figs. 2b–2d), particularly of the large cation occupying the 3*e* site toward the cavity (Fig. 2c, on the left). Interestingly, the O3(6*g*) atoms, which form electric dipoles with the 3*e* cation under an applied pressure along the *a* axis, move in a direction almost perpendicular to the movement of the 3*e* cation (Fig. 2c). These observations confirm the fact that the 3*e*-cation–O3(6*g*) bond is relatively weak and support the conclusions [12, 13] about the role of the 3*e* cation in the manifestation of piezoelectric properties of the langasite family crystals.

Changes in the series CTGS → STGS → BTGS correlate with the size of the 3*e* cation and are more

Table 1. Crystallographic characteristics and the X-ray data collection and structure refinement statistics for $Ba_3TaGa_3Si_2O_{14}$

Experiment	I	II	III	IV
T, K	295	295	106	106
Crystal sizes determined with an optical microscope, mm	0.23–0.26			
Calculated crystal size, mm	0.229(1), 0.247(1), 0.259(1)	0.229(1), 0.244(1), 0.258(1)	0.232(1), 0.240(1), 0.271(1)	0.232(1), 0.244(1), 0.267(1)
Crystal system, sp. gr., Z	Trigonal, $P321$, 1			
a, c, Å	8.51690(2), 5.19163(1)	8.51473(2), 5.19047(1)	8.51178(5), 5.18705(3)	8.51002(5), 5.18520(3)
V, Å^3	326.135(3)	325.896(4)	325.456(3)	325.205(3)
μ, mm^{-1}	23.78		23.76	
α*, K^{-1}	$\|a$: 0.288×10^{-5}; $\|c$: 0.475×10^{-5}			
Diffractometer	Xcalibur S			
Radiation; λ, Å	MoK_α; 0.71073			
θ_{max}, deg	71.9	74.0	74.1	74.2
Limiting indices h, k, l	$-22 \le h \le 20$, $-22 \le k \le 22$, $-13 \le l \le 13$	$-19 \le h \le 20$, $-22 \le k \le 22$, $-13 \le l \le 14$	$-22 \le h \le 20$, $-22 \le k \le 22$, $-13 \le l \le 14$	$-22 \le h \le 20$, $-23 \le k \le 22$, $-14 \le l \le 13$
Number of reflections: measured/unique with $F^2 < 2\sigma(F^2)$	52193/4270	50776/4425	33505/4299	33487/4329
Number of discarded unique reflections, $F^2 < 2\sigma(F^2)$	91	65	98	77
Redundancy	11.97	11.31	7.48	7.49
$\langle\sigma(F^2)/F^2\rangle$	0.018	0.016	0.019	0.020
$R1_{aver}(F^2)/wR2_{aver}(F^2)$, %	2.14/3.49	2.16/3.15	2.98/4.31	2.52/3.23
Refinement based on cross-data sets				
Number of reflections and parameters	4414/104		4382/103	
$R12_{aver}(\|F\|)/wR12_{aver}(\|F\|)$, %	0.498/0.451		0.923/2.218	
$R1(\|F\|)/wR2(\|F\|)$, %	0.578/0.562		0.754/0.855	
S	0.967		0.853	
$\Delta\rho_{min}/\Delta\rho_{max}$, e/Å^3	–0.73/0.42		–0.81/1.06	

The following programs were used: CrysAlisPro [22], ASTRA [24]. $\langle a\rangle$ = 8.516(1) Å, $\langle c\rangle$ = 5.1910(6) Å at 295 K; $\langle a\rangle$ = 8.5109(9) Å, $\langle c\rangle$ = 5.1861(9) Å at 106 K; * $\alpha = (1/\langle p\rangle) \cdot (\Delta p/\Delta T)$ is the coefficient of linear expansion in the temperature range ΔT 106–295 K, p is the unit-cell parameter a or c; $R12_{aver}$ is the R factor for averaging identical reflections from two data sets after merging together into the cross-data set; $R1(|F|) = \Sigma\||F_{obs}| - |F_{calc}|\|/\Sigma|F_{obs}|$; $wR2(|F|) = \sqrt{\{\Sigma w(|F_{obs}| - |F_{calc}|)^2/\Sigma w(F_{obs})^2\}}$.

Table 2. Atomic coordinates, site occupancies Q, equivalent thermal displacement parameters U_{eq}, and ellipsoidalities ε of atomic displacements in the $Ba_3TaGa_3Si_2O_{14}$ crystal at 295 K (upper row) and 106 K (lower row)

Atom	Site	*x/a*	*y/b*	*z/c*	*Q*	U_{eq}, Å^2	ε
Ba	3*e*	0.43232(1) 0.43202(2)	0	0	1.0	0.011101(6) 0.00567(1)	0.0047 0.0038
Ta	1*a*	0	0	0	1.0	0.00931(6) 0.0054(1)	0.0023 0.0005
Ga	3*f*	0.74621(2) 0.74614(4)	0	1/2	1.0	0.00915(8) 0.0056(8)	0.0132 0.0138
Si	2*d*	1/3	2/3	0.51822(8) 0.51929(8)	1.0	0.0086(3) 0.0041(1)	0.0004 0.0003
O1	2*d*	1/3	2/3	0.2110(1) 0.2118(2)	1.0	0.0133(5) 0.0070(1)	0.0121 0.0075
O2	6*g*	0.47358(1) 0.47322(9)	0.2983(1) 0.2979(3)	0.3557(2) 0.3534(3)	1.0	0.01373(7) 0.00826(9)	0.0227 0.0114
O3	6*g*	0.21721(5) 0.21737(9)	0.10649(6) 0.10602(8)	0.77459(7) 0.77441(9)	1.0	0.01420(7) 0.00753(8)	0.0285 0.0177

complicated for BTFS containing magnetic Fe^{3+} ions at the 3*f* site as compared to BTGS. An increase in the volume of the Fe(3*f*) tetrahedron causes a contraction of the small Si(2*d*) tetrahedron, which is located to the left of the former tetrahedron in the same level at $z \sim 1/2$, and the rotation of the O3(6*g*) atoms (Figs. 2a and 2b). An additional rotation of the atoms along the line of the triple-thread structural helix Fe(3*f*)–O3(6*g*)–O3(6*g*)–Fe(3*f*) is observed. The rotation of the O3(6*g*) atoms in different directions is clearly seen for the 1*a* octahedron (Fig. 2d).

Therefore, an increase in the internal pressure due to the sequential insertion of ever-larger cations in the 3*e* site is accompanied by an increase in the compactness of the helix. The Ga(3*f*) → Fe(3*f*) substitution not only enhances this effect but also leads to an increase the degree of helix twist. Almost linear changes in the atomic positions are observed in the series CTGS → STGS → BTGS. However, specific features in the atomic positions appear upon the BTGS → BTFS transformation, which can be attributed to indirect magnetic exchange coupling that occurs in BTFS [17] but is absent in the former three crystals.

CONCLUSIONS

An accurate X-ray diffraction study of the langasite family BTGS structure gave results with high relative precision (sp. gr. *P*321, $Z = 1$, $\sin\theta/\lambda \le 1.35$ Å^{-1}; at 295 K $a = 8.516(1)$ Å, $c = 5.1910(6)$ Å, $R/wR = 0.58/0.56\%$, $\Delta\rho_{min}/\Delta\rho_{max} = -0.73/0.42$ e/Å^3, 4414 independent reflections; at 106 K $a = 8.5109(9)$ Å, $c = 5.1861(9)$ Å, $R/wR = 0.75/0.86\%$, $\Delta\rho_{min}/\Delta\rho_{max} = -0.81/1.06$ e/Å^3, 4382 reflections). The high quality of the study was achieved due to the use of high-resolution experimental data, application of specials data-processing methods, and high redundancy. The structural specific feature of $Ba_3TaGa_3Si_2O_{14}$ is an anharmonic character of the motion of four cations, particularly of Ga(3*f*), and one oxygen atom

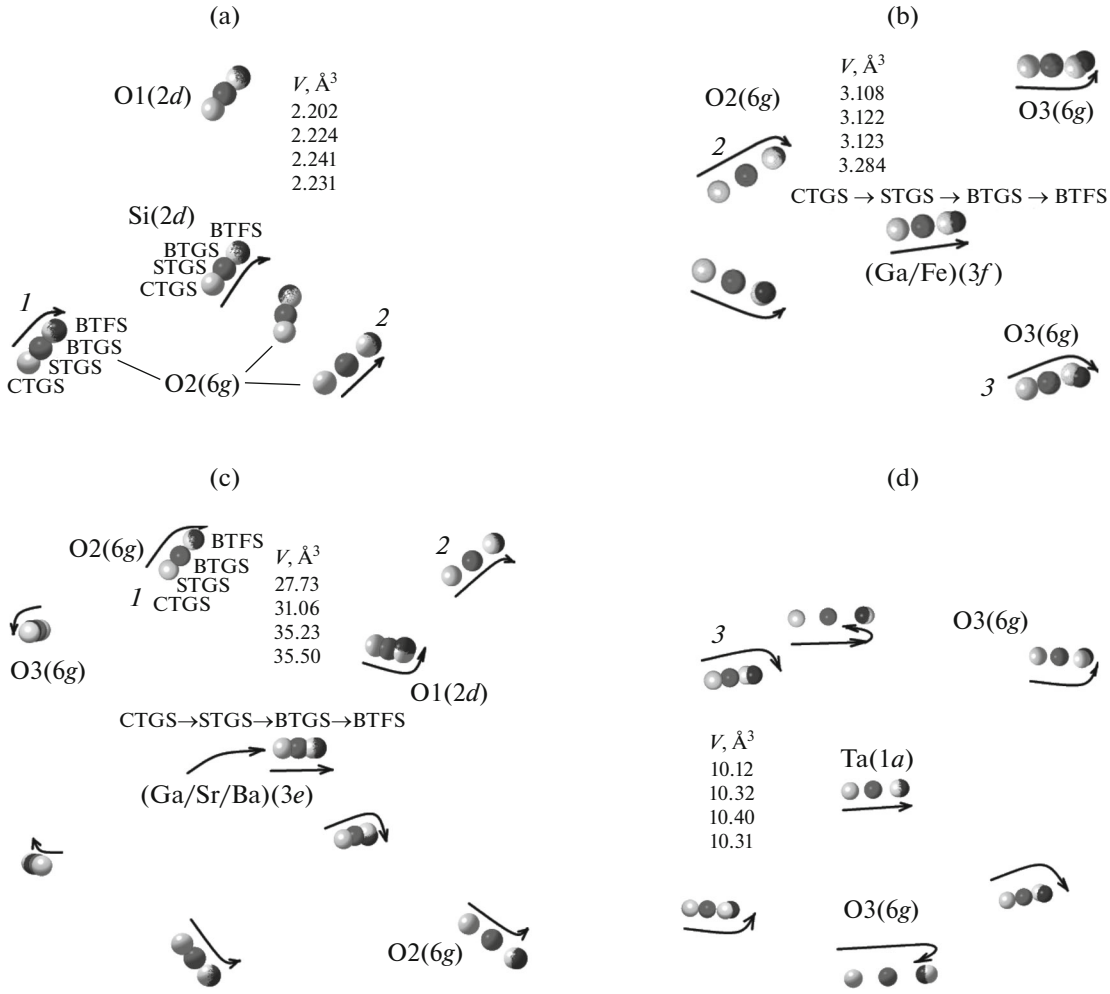

Fig. 2. Scheme of atom movements caused by isomorphous substitutions in the series CTGS → STGS → BTGS → BTFS: (a) a silicon tetrahedron at the 2*d* site moves upward; (b) a 3*f* tetrahedron moves toward the axis of the structural helix; in BTFS the O3(6*g*) atoms additionally rotate along the axis of the helix; (c) a 3*e* polyhedron is expanded upon rotation of O3(6*g*); (d) a change in rotation of the O3(6*g*) atoms upon the BTGS → BTFS transformation observed in the tantalum octahedron at the 1*a* site. The arrangement and orientation of the polyhedra correspond to those shown in Fig. 1. The "transformations" of two O2(6*g*) atoms and one O3(6*g*) atom in the series of the crystals under consideration are marked with the numbers *1*, *2*, and *3*.

occupying a general position. These data were employed for a comparative analysis of the $Ca_3TaGa_3Si_2O_{14}$, $Sr_3TaGa_3Si_2O_{14}$, $Ba_3TaGa_3Si_2O_{14}$, and $Ba_3TaFe_3Si_2O_{14}$ crystals. The structural mechanism of piezoelectricity of langasite family crystals was confirmed. The isomorphous substitutions under consideration were shown to give rise to a more compact and twisted atomic helix, which is a structural basis for magnetic ordering in the $Ba_3TaFe_3Si_2O_{14}$ crystal.

ACKNOWLEDGMENTS

I am grateful to B.V. Mill' for supplying crystals.

This work was supported by the Federal Agency of Scientific Organizations (agreement no. 007-ГЗ/Ч3363/26) and was carried out within the framework of the research project 0026-2014-0001 using equipment of the Shared Research Center of the Shubnikov Institute of Crystallography of Federal Scientific Research Centre "Crystallography and Photonics" of the Russian Academy of Sciences.

REFERENCES

1. P. Hohenberg and W. Kohn, Phys. Rev. B **136**, 864 (1964).
2. W. Kohn and L. J. Sham, Phys. Rev. A **140**, 1133 (1965).
3. S. Baroni, P. Giannozzi, and A. Testa, Phys. Rev. Lett. **58**, 1861 (1987).
4. X. Gonze, Phys. Rev. B **52**, 1086 (2005).
5. E. Espinosa, I. Alkorta, I. Rosas, et al., Chem. Phys. Lett. **336**, 457 (2001).
6. E. L. Belokoneva and N. V. Belov, Dokl. Akad. Nauk SSSR **260** (6), 1363 (1981).

7. B. V. Mill and Yu. V. Pisarevsky, *Proc. 2000 IEEE/EIA Intern. Frequency Control Symp. Kansas City, Missouru, USA,* p. 133.
8. A. A. Kaminskii, E. L. Belokoneva, B. V. Mill, et al., Phys. Status Solidi A **86**, 345 (1984).
9. E. L. Belokoneva, S. Yu. Stefanovich, Yu. V. Pisarevskii, et al., Zh. Neorg. Khim. **45** (11), 1786 (2000).
10. V. Yu. Ivanov, A. A. Mukhin, A. S. Prokhorov, and B. V. Mill, Solid State Phenom. **152–153**, 299 (2009).
11. H. D. Zhou, L. L. Lumata, P. L. Kuhns, et al., Chem. Mater. **21**, 156 (2009).
12. N. Araki, H. Oshato, K. Kakimoto, et al., J. Eur. Ceram. Soc. **27**, 4099 (2007).
13. A. P. Dudka and V. I. Simonov, Crystallogr. Rep. **56** (6), 980 (2011).
14. A. P. Dudka and B. V. Mill, Crystallogr. Rep. **58** (4), 594 (2013).
15. A. P. Dudka and B. V. Mill, Crystallogr. Rep. **59** (5), 689 (2014).
16. A. F. Konstantinova, T. G. Golovina, B. V. Nabatov, et al., Crystallogr. Rep. **60** (6), 907 (2015).
17. S. A. Pikin, I. S. Lyubutin, and A. P. Dudka, Crystallogr. Rep. **60** (5), 729 (2015).
18. A. P. Dudka, Crystallogr. Rep. **61** (2), 187 (2016).
19. A. P. Dudka and B. V. Mill', Crystallogr. Rep. **56** (3), 443 (2011).
20. A. P. Dudka, A. M. Balbashov, and I. S. Lyubutin, Crystallogr. Rep. **61** (1), 24 (2016).
21. A. P. Dudka, I. A. Verin, and E. S. Smirnova, Crystallogr. Rep. **61** (4), 692 (2016).
22. *Rigaku Oxford Diffraction, CrysAlisPro Software System, Version 1.171.38.41* (Rigaku, Oxford, UK, 2015).
23. A. P. Dudka, Crystallogr. Rep. **47** (1), 152 (2002).
24. A. Dudka, J. Appl. Crystallogr. **40**, 602 (2007).
25. A. P. Dudka, M. Kh. Rabadanov, and A. A. Loshmanov, Kristallografiya **34** (4), 818 (1989).
26. A. P. Dudka, Crystallogr. Rep. **57** (1), 131 (2012).
27. A. P. Dudka, Crystallogr. Rep. **50** (6), 1068 (2005).
28. A. Dudka, J. Appl. Crystallogr. **43** (6), 1440 (2010).
29. A. P. Dudka, Crystallogr. Rep. **60** (4), 601 (2015).
30. P. J. Becker and P. Coppens, Acta Crystallogr. A **30**, 129 (1974).
31. Page. Y. Le and E. J. Gabe, J. Appl. Crystallogr. **11**, 254 (1978).
32. A. Dudka, J. Appl. Crystallogr. **43**, 27 (2010).
33. W. C. Hamilton, Acta Crystallogr. **18**, 502 (1965).
34. S. C. Abrahams and E. T. Keve, Acta Crystallogr. A **27**, 157 (1971).
35. A. P. Dudka, Crystallogr. Rep. **47** (1), 145 (2002).

Translated by T. Safonova